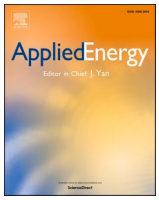
Applied Energy 420 (2026) 128142



Contents lists available at ScienceDirect

Applied Energy

journal homepage: www.elsevier.com/locate/apenergy



Quantum-enhanced forecasting and optimal scheduling for energy management in photovoltaic greenhouses

Zhenhao Weng [a,1], Zhanpeng Xu [a,1], Ruichong Li [a], Longze Wang [a,*], Zhehan Li [a], Yan Zhang [b,c], Meicheng Li [a,*]

[a] State Key Laboratory of Alternate Electrical Power System With Renewable Energy Sources, School of New Energy, North China Electric Power University, Beijing 102206, China
[b] School of Economics and Management, North China Electric Power University, Beijing 102206, China
[c] Beijing Key Laboratory of New Energy and Low-Carbon Development, Beijing 102206, China

HIGHLIGHTS

- Energy management method based on variational quantum algorithm for PV greenhouses is proposed.
- A DAM-QLSTM model improves forecasting accuracy for energy supply and demand in complex greenhouse environments.
- A VQC-based optimization model is developed to address the non-convex optimization problem with multi-physics constraints.
- Beijing PV greenhouse tests confirm the practical effectiveness of quantum algorithms.

ARTICLE INFO

Keywords:
Energy management
Quantum computing
Photovoltaic greenhouses
Energy forecasting
Optimal scheduling

ABSTRACT

Photovoltaic (PV) greenhouses represent a promising pathway toward sustainable agriculture by enabling clean energy utilization and improving crop productivity. However, their energy management is constrained by two critical challenges: the uncertainty in energy supply and demand, and the complexity of non-convex optimization. This paper proposes a novel energy management method based on variational quantum algorithms. Firstly, a quantum machine learning forecasting model, namely a dual attention mechanism-based quantum long short-term memory (DAM-QLSTM), is developed to improve the prediction accuracy by exploiting its expressive capacity for modeling nonlinear dependencies. Secondly, based on the prediction results, a variational quantum circuit (VQC)-based rolling optimization model is formulated to address the non-convex optimization problem with multi-physics constraints, leveraging quantum interference to improve exploration of the solution space. Finally, the proposed DAM-QLSTM-VQC method is validated using practical data from a PV greenhouse in Beijing, demonstrating a 9.6% improvement in renewable energy utilization compared with particle swarm optimization, along with reductions in total operating cost, carbon and pollutant emissions. Compared with model predictive control, the proposed method reduces cost by 1.5% and emissions by 4.7%. These findings highlight the potential of quantum computing to enhance the energy management efficiency in complex agricultural energy systems.

1. Introduction

The global population had reached approximately 8.2 billion and is projected to surpass 10 billion by the middle of this century. The constrained nonlinear growth of the global population poses increasingly severe challenges to agricultural systems worldwide [1]. Meanwhile, as public awareness and demand for renewable energy continue to rise, photovoltaic (PV) power generation has experienced rapid development. Because of its inherent intermittency and variability, the utilization efficiency of PV power remains relatively low [2]. PV greenhouses, which integrate PV generation with traditional greenhouse agriculture,

* Corresponding authors.
E-mail addresses: 120252111026@ncepu.edu.cn (Z. Weng), 120222111030@ncepu.edu.cn (Z. Xu), 120242211004@ncepu.edu.cn (R. Li), lzwang@ncepu.edu.cn (L. Wang), 120232111033@ncepu.edu.cn (Z. Li), zhangyan8698@ncepu.edu.cn (Y. Zhang), mcli@ncepu.edu.cn (M. Li).
[1] These authors contributed equally.

https://doi.org/10.1016/j.apenergy.2026.128142
Received 14 January 2026; Received in revised form 11 April 2026; Accepted 27 May 2026
0306-2619/© 2026 Published by Elsevier Ltd.

Nomenclature

Abbreviations

DAM	Dual attention mechanism
ESS	Energy storage system
FAM	feature attention mechanism
LSTM	long short-term memory network
MAE	Mean Absolute Error
MSE	Mean Squared Error
MTAM	Multi-head temporal attention mechanism
PSO	Particle swarm optimization
PV	Photovoltaic
QA	Quantum annealing
QAOA	Quantum approximate optimization
QLSTM	Quantum long short-term memory network
QUBO	Quadratic unconstrained binary optimization
RMSE	Root Mean Squared Error
RNN	Recurrent Neural Network
SA	Simulated annealing
VQAs	Variational quantum algorithms
VQC	Variational quantum circuit

Parameters

A_{gh}	Greenhouse area
A_{pv}	Surface area of PV modules
C	Available battery capacity
ΔC	Degraded battery capacity
$C_{battery}$	Battery capacity
C_{buy}	Electricity purchasing cost
C_d	Resistance coefficient
$CNOT$	Controlled-NOT gate
C_{ES}	Battery degradation cost
C_{sell}	Electricity selling income
C_{total}	Total operational cost
C_0	Nominal capacity of battery
E_{pollut}	Pollutant emission
f	Total objective function
f_{pv}	Fill factor
$\frac{\partial f}{\partial \theta}$	Quantum gradient
$f_{weather}$	Influence of weather conditions
G	Solar irradiance
$\mu(\theta)$	Expectation vector
H_{in}	Internal humidity
H_{out}	External humidity
k_{cell}	Temperature coefficient
k_t	Heat transfer coefficient
L_{am}	Required light intensity for crop
m_{air}	Air quality flow
N_{cyc}	Number of battery cycles
$P_{pv\rightarrow load}$	Power from PV to greenhouse
$P_{pv\rightarrow ES}$	Power from PV to ESS
$P_{pv\rightarrow grid}$	Power from PV to power grid
$P_{ES\rightarrow load}$	Power from ESS to greenhouse
$P_{ES\rightarrow grid}$	Power from ESS to power grid
$P_{grid\rightarrow load}$	Power from power grid to greenhouse
$P_{grid\rightarrow ES}$	Power from power grid to ESS
$P_{ij,t}, Q_{ij,t}$	Active and reactive power of line ij at time t
$p_{j,t}, q_{j,t}$	Net injected active and reactive power at bus j and time t
P_c	Load of the cooling system
P_{load}	Total load of the PV greenhouses
P_{grid}	Grid output power
P_h	Load of the heating system
P_{supply}	Actual supplied power
$P_{ES}^{charg}/P_{ES}^{disch}$	Charging and discharging power of battery
P_l	Load of the lighting system
P_m	Load of agricultural machinery
P_{pv}	Output power of PV system
P_{ES}	Energy storage system output power
P_v	Load of the ventilation system
R_x, R_y, R_z	Rotation-X/Y/Z gate
$S(t)$	Solar light intensity at time t
SOC	State of charge
T	Total time horizon
T_{am}	Optimal temperature for plant growth
T_{cell}	PV cell temperature
T_{in}	Internal temperature of the greenhouse
T_{out}	External temperature
T_{ref}	Standard temperature
ΔT	Time interval
ub, lb	Upper/lower bound of unknown variable
v	Ventilation speed
$\boldsymbol{x}(\theta)$	Decision variable vector
Z_n	Pauli-Z operator
θ	Quantum circuit parameters
ϕ	Charging/discharging efficiency of battery
Φ_{grow}	Plant growth loss
$\|\varphi_0\rangle$	Initial quantum state
$\lambda_{sell}/\lambda_{buy}$	Daily electricity selling/purchasing price
γ	Natural light utilization coefficient
η_{bat}	Capacity loss coefficient
η_c	Cooling efficiency
η_{de}	Battery degradation efficiency
η_h	Heating efficiency
η_{pv}	Photoelectric conversion efficiency
η_{re}	Utilization rate of renewable energy
η_v	Fan efficiency
δ_{conv}	Efficiency of battery power converter

offers the dual benefits of enhancing crop yields and promoting local consumption of renewable energy, making it a promising solution for sustainable agriculture [3]. With the expansion of the scale of PV greenhouses and the increasing complexity of their integrated energy demands, the development of efficient energy management methods has become more important than ever.

The energy management in PV greenhouses is a typical non-convex optimization problem with uncertainty [4]. In this system, PV generation, energy storage, and interactions with the power grid constitute a complex multi-energy flow process. These processes are simultaneously constrained by multiple factors, including dynamic energy balance, mutual exclusivity of charging and discharging, and battery capacity limits. Meanwhile, both PV generation and greenhouse energy demand exhibit significant uncertainty and volatility, further increasing the complexity of system optimization [5]. Moreover, Classical approaches typically employ linear programming to address single linear objectives, such as total operating cost. However, with growing emphasis on environmental and ecological considerations, the objective functions in PV greenhouses energy management have become more complex, frequently non-linear and even non-convex [6]. When solving this problem, classical algorithms project the solution space into lower-dimensional and discontinuous regions, which easily trap algorithms

in local optima [7].

Quantum computing offers a novel solution to the non-convex optimization problem [8]. As a computational paradigm based on the principles of quantum mechanics, quantum computing leverages properties such as superposition and entanglement to significantly enhance computational capabilities when addressing complex tasks. Currently, variational quantum algorithms (VQAs) which combine parameterized quantum circuits with classical optimizer, have emerged as a promising hybrid framework [9]. Represented by the quantum annealing (QA) [10] and quantum approximate optimization algorithm (QAOA) [11], VQAs address combinatorial optimization problem by formulating them as Quadratic Unconstrained Binary Optimization (QUBO) model and solving them using quantum computers [12–13]. Existing study shows that this method can improve the efficiency and performance in building demand response challenge [14]. However, in practice, energy management is not a simple combinatorial optimization problem and therefore cannot be formulated as a QUBO model and solved directly using QA or QAOA [15]. The application of VQAs to address non-convex optimization problem under multiple uncertainties remains an open and underexplored research gap in PV greenhouses energy management.

To address the aforementioned research gaps, we propose a quantum-enhanced energy management method for PV greenhouses in this study, named DAM-QLSTM-VQC.

First, facing the dual uncertainties of PV generation and greenhouse load, we propose a dual attention mechanism-based quantum long short-term memory (DAM-QLSTM) forecasting model integrates quantum and machine-learning frameworks. The model leverages quantum structure to capture the nonlinear and dynamic coupling within the input dataset, thereby providing more accurate power forecasts for operational optimization. Second, we introduce a novel variational quantum circuit (VQC)-based rolling optimization model. By mapping the expectation values of Pauli-Z operators to physical variables, the original complex non-convex optimization problem is reformulated into a differentiable parameterized form, enabling quantum gradient-based optimization by quantum circuit. Leveraging this optimization foundation, the rolling model dynamically formulates scheduling decisions by integrating PV generation and load forecasts. The main contributions are summarized as follows:

- A dual attention mechanism-based quantum long short-term memory (DAM-QLSTM) forecasting model seamlessly integrates quantum and machine-learning frameworks to deliver more accurate power forecasts for operational optimization.
- An original variational quantum circuit (VQC)-based rolling optimization model, based on prediction result, is developed to address the complex non-convex optimization problem under multiple objectives and constraints, significantly improving the efficiency of PV greenhouses.
- The proposed DAM-QLSTM-VQC method is validated with actual data from a typical PV greenhouse in Beijing, showing significant improvements in energy efficiency. Comparative analyses with conventional methods further highlight the advantages of quantum computing in managing complex energy systems.

The rest of this paper is organized as follows: Section 2 reviews the related literature of energy management in PV greenhouses and the quantum computing. Section 3 presents the modeling of PV greenhouses, including the system architecture, energy management framework, and associated constraints. Section 4 introduces the detailed design and implementation of the proposed strategy, DAM-QLSTM-VQC. In Section 5, a case study based on a PV greenhouse in Beijing is conducted. Finally, Section 6 concludes the paper with a summary of the main findings.

2. Literature review

As an introduction to our study, we review the related literature in two areas: energy management in PV greenhouses and the quantum computing.

2.1. Energy management in PV greenhouses

With the widespread adoption of PV greenhouses, research on energy management has increased significantly. Various mathematical programming and heuristic algorithms have been employed to address the energy management problem in PV greenhouses, including Linear Programming methods, particle swarm optimization (PSO), genetic algorithm (GA), and simulated annealing (SA) [16]. For example, Ref. [17] employed particle swarm optimization as a demand-side management method in PV greenhouses, enabling time-shifted power scheduling that improved energy utilization and boosted the economic performance of greenhouse operations. Ref. [4] proposed a Hierarchical optimization framework for PV greenhouses based on the sequential quadratic programming algorithm, which effectively reduced overall operational costs.

Moreover, with the rapid development of artificial intelligence technologies in recent years, machine learning methods have played an increasingly important role in the energy management of PV greenhouses [18–19]. In the forecasting field, many researches exploit machine learning to improve prediction accuracy, such as long short-term memory (LSTM) network and attention mechanism. Ref. [20] developed a Transformer-based model for solar irradiance prediction in PV greenhouses, which achieved high accuracy and strong generalization across varying time steps, seasons, and weather conditions. Ref. [21] proposed a robust model predictive control (MPC) framework for PV greenhouses, incorporating machine learning-based uncertainty sets, which improved renewable energy usage efficiency to 127.5% and increased crop yield to 16.1 wt%. In the optimization field, reinforcement learning becomes essential. Ref. [22] introduced a multi-agent deep reinforcement learning control framework for demand-side energy management in a network of renewable energy integrated greenhouses, which can ensure a 28% reduction in net load demand as compared to well-known algorithms.

Existing machine learning and heuristic optimization technologies have contributed to improvements in PV greenhouses energy management. Nevertheless, they still encounter difficulties in addressing large-scale, time-critical, and strongly coupled decision problems, particularly in terms of generalization, dynamic constraint modeling, and convergence reliability [23].

2.2. The quantum computing

The emergence of quantum computing technology has provided a new perspective for solving constrained nonlinear optimization problems. Quantum computing demonstrates inherent advantages in optimization, particularly through its ability to perform parallel searches in exponential solution spaces [24]. In recent years, researchers have begun exploring various applications of quantum computing in energy systems, including power flow analysis [25], capacity optimization [26], load forecasting [27], and fault diagnosis and recovery in complex power grids [28], achieving some promising initial results. For example, in power flow analysis, quantum computing can leverage its strong parallel processing capabilities to efficiently solve large-scale linear equations, thereby improving the real time performance and stability of power system operations [29]. In capacity planning and optimization, quantum algorithms can rapidly identify near-optimal solutions within high-dimensional search spaces, enhancing energy allocation and grid capacity configuration, and ultimately improving system efficiency and reliability [30].

By integrating VQAs with machine learning, researchers have further

extended the application scope [31,32]. In power forecasting, the quantum long short-term memory (QLSTM) model incorporates quantum computing into the LSTM model, enabling the optimization of gate parameters and significantly improving prediction accuracy over traditional methods [33]. Moreover, VQAs exhibits strong adaptability in handling nonlinear constraints and complex objective functions [12], making them particularly suitable for optimization tasks in energy management. Gradient-based optimization, where gradients are estimated through quantum measurements, has been recognized as a promising parameter training method for quantum neural networks [34]. Despite rapid progress in applying quantum computing to the energy sector, further research is still needed to identify feasible and effective approaches for improving energy management efficiency.

In summary, most existing research on PV greenhouses energy management still relies on traditional optimization methods, with limited exploration of quantum computing approaches. Table 1 summarizes representative recent research on energy management methods applied in PV greenhouses. Meanwhile, current studies applying quantum algorithms are predominantly published in the fields of physics or quantum information science, rarely addressing practical engineering problems such as energy management in practical energy systems. Only a few recent works in energy economics or power system optimization have touched upon quantum heuristic methods, but they typically do not consider the complex and uncertain environment of PV greenhouses.

The main contribution of this paper is to propose a novel energy management method based on VQAs. By leveraging the hybrid quantum-classical architecture, the proposed method enables efficient handling of complex non-convex optimization problem. Unlike conventional energy management methods, the proposed method leverages the entanglement and parallelism capabilities of quantum computing to capture complex correlations and explore high-dimensional solution spaces efficiently, thereby improving the energy management efficiency of PV greenhouses.

3. PV greenhouses system framework

3.1. System composition

The structure of the PV greenhouses system is illustrated in Fig. 1. It consists of four core components: the PV system, energy storage system, distribution grid, and greenhouse loads. The PV modules are typically installed in a distributed layout on the greenhouses' rooftop glazing surfaces. They convert solar radiation into electrical energy through the PV effect, thereby meeting the daily energy demands of the greenhouses [35]. When excess electricity is generated during peak PV output periods, it can be stored in the energy storage system for future use or sold to the grid to enhance economic efficiency. When PV generation is insufficient, the stored energy is discharged to bridge the gap between energy supply and demand. If both PV output and storage capacity fall short of meeting the load requirements, additional electricity is purchased from the distribution grid to maintain optimal growing conditions for the plants inside the greenhouses.

Table 1
Comparative analysis of typical methods.

Ref.	Cost	Efficiency	Supply-demand uncertainty	Pollution emission	Method
Zhang et al. [13]	✓	×	×	×	heuristic
Lin et al. [4]	✓	×	×	✓	nonlinear programming
Zhu et al. [16]	×	×	✓	×	machine learning
Hu et al. [17]	✓	✓	×	×	machine learning
Ajagekar et al. [18]	✓	×	✓	×	machine learning
DAM-QLSTM-VQC	✓	✓	✓	✓	quantum computing

3.1.1. Energy consumption

The greenhouse energy model captures the dynamic variations in energy consumption, which primarily arise from the operation of environmental control systems, such as heating, cooling, lighting, ventilation, and auxiliary agricultural machinery. These energy demands exhibit pronounced temporal and seasonal fluctuations [36]. Under cold conditions, the heating system maintains optimal internal temperatures, with electricity demand increasing as ambient temperature decreases, as shown in Eq. (1). During high-temperature periods, the cooling system operates to regulate thermal conditions, and its power consumption is closely related to air temperature and humidity, as described in Eq. (2). When natural light is insufficient to support photosynthesis, the lighting system provides supplemental illumination. Its power demand varies with solar radiation intensity and plant growth stages, as modeled in Eq. (3). The ventilation system regulates humidity and CO_2 concentration, and its energy consumption depends on ventilation speed and fan efficiency, as indicated in Eq. (4). In addition, energy consumption by agricultural machinery depends on production requirements and the degree of automation, accounting for a substantial portion of the total energy use. These diverse energy demands are dynamically balanced in the overall energy consumption model to ensure optimal energy allocation throughout various seasons and growth stages. The total energy demand is represented by Eq. (5).

$$P_h(t) = \frac{k_t \bullet A_{gh} \bullet (T_{in} - T_{am})}{\eta_h} \tag{1}$$

$$P_c(t) = \frac{k_t \bullet A_{gh} \bullet (T_{am} - T_{in})}{\eta_c} \tag{2}$$

$$P_l(t) = A_{gh} \bullet [L_{am} - \gamma \bullet S(t)] \tag{3}$$

$$P_v(t) = \frac{m_{air} \bullet \nu \bullet C_d}{\eta_v} \tag{4}$$

$$P_{load}(t) = P_h(t) + P_c(t) + P_l(t) + P_v(t) + P_m(t) \tag{5}$$

3.1.2. PV power generation

By converting solar energy into electricity, the PV system powers environmental control devices and agricultural machinery in the greenhouses or charges the energy storage system. The amount of electricity generated by the PV system is influenced by several factors, including solar irradiance, the conversion efficiency of the PV modules, and the surface area of the installed panels. The output power of the PV system is determined by the module surface area, conversion efficiency, and fill factor, where the fill factor reflects the density of PV module arrangement within the system. Given the solar irradiance, the PV system output power is calculated according to Eqs. (6)–(8) [37].

$$P_{pv}(t) = \eta_{pv} \bullet A_{pv} \bullet f_{pv} \bullet f_{weather}(t) \tag{6}$$

$$f_{weather}(t) = G(t) \bullet \left(1 + k_{cell} \bullet \left(T_{cell}(t) - T_{ref}(t)\right)\right) \tag{7}$$

$$T_{cell}(t) = T_{out}(t) + 0.0256 \times G(t) \tag{8}$$

3.1.3. Energy storage

The energy storage system serves as a core regulatory component within the PV greenhouses, primarily functioning to mitigate the intermittent fluctuations of PV generation. Specifically, by Leveraging the battery's rapid response characteristics, the system compensates in real time for the power load variations within the greenhouses. During

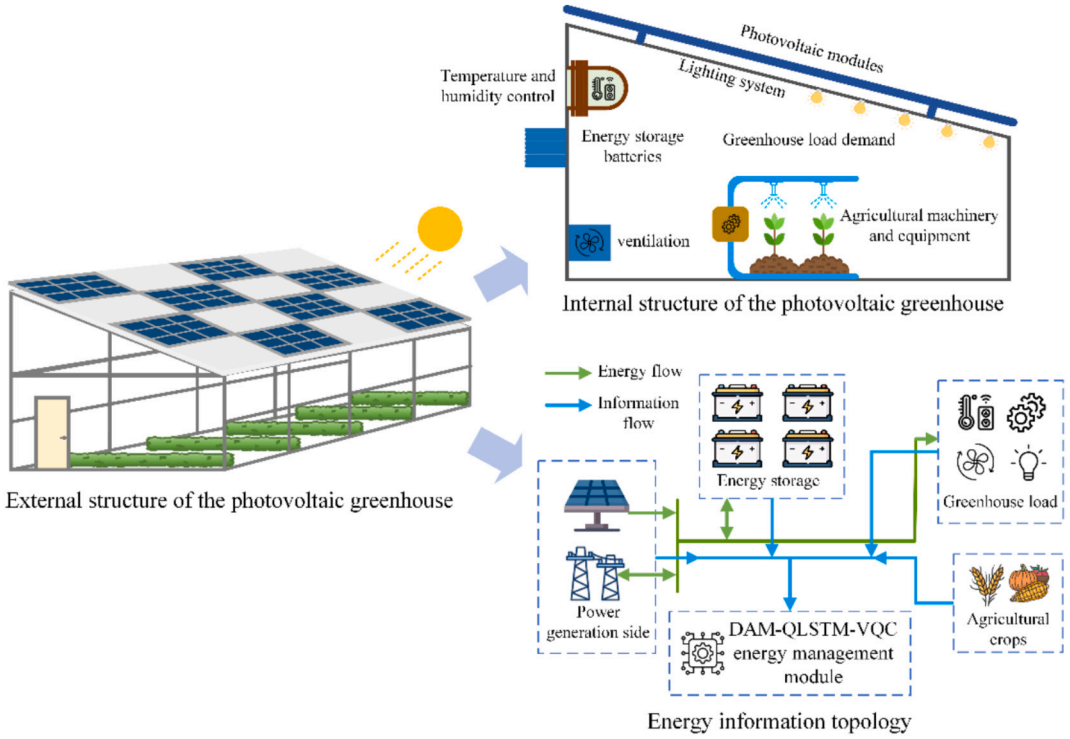


Fig. 1. Structural schematic diagram of the PV greenhouses.

periods of low demand, excess electricity is stored, and during peak demand periods, stored energy is discharged to maintain a dynamic balance between power supply and consumption. The characteristics of the storage battery can be described by its nominal capacity, real-time capacity, and charge/discharge efficiency [38]. The nominal capacity refers to the battery's rated capacity under initial conditions. The capacity loss coefficient measures the extent of degradation in each work cycle. The change in the battery's state of charge (SOC) can be described by Eq. (9), while the battery power is expressed in Eq. (10). Due to degradation, the battery capacity decreases over time. The degradation value is determined by the capacity loss coefficient and the number of cycles, as shown in Eq. (11).

$$SOC(t+1) = SOC(t) - \frac{\Delta T \times P_{ES}^{disch}(t) \times \phi^{disch}}{\delta_{conv} \times C(t)} + \frac{\Delta T \times \delta_{conv} \times P_{ES}^{charg} \times \phi^{charg}}{C(t)} \tag{9}$$

$$P_{ES} = P_{ES}^{disch} - P_{ES}^{charg} \tag{10}$$

$$C(t+1) = C(t) - \Delta C(t) = \left(1 - \eta_{bat} \times N_{cyc}(t)\right) \times C(t) \tag{11}$$

3.1.4. Power grid

In the energy management system of the PV greenhouses, the power grid serves as a backup energy source to ensure stable operation when PV generation and the energy storage system are insufficient to meet the demand. Based on the current state of charge, when both PV generation and battery output fail to satisfy the greenhouse demand, the system compensates for the deficit by purchasing electricity from the grid, thereby maintaining continuous operation and a stable growing environment. The electrical power supplied by the grid is calculated by Eq. (12). In addition to electricity costs, the environmental impact associated with grid electricity consumption is taken into account. For each kWh of electricity consumption from the grid, an estimated emission of 1.13 kg of CO_2, 9.61 $\times$ 10^{-3} kg of SO_2, and 2.83 $\times$ 10^{-3} kg of NO_x is produced in Eq. (13) [39].

$$P_{grid}(t) = P_{load}(t) - P_{pv}(t) - P_{ES}(t) \tag{12}$$

$$E_{pollut} = \frac{O_{coal} \times h_{coal} \times \mu_{pollut}}{E_{elec}} \tag{13}$$

where the heating value of standard coal is $h_{coal} = 2.93 \times 10^7$ J/kg. μ_{pollut} is the pollutant emission per unit energy. The oxidization rate of coal is set as $O_{coal} = 99\%$. The power generation per ton of coal is $E_{elec} = 2475$ kWh [40].

3.2. Optimization objective

There are three primary objectives: minimizing operational costs, maximizing the utilization of renewable energy and minimizing plant growth loss [4]. Specifically, the cost minimization objective seeks to reduce the operational expenses, as formulated in Eq. (14). These expenses include the electricity purchase cost, the electricity selling revenue, and the battery degradation cost in Eqs. (15)–(17). For short-term management, we simplified the cost function by omitting investment and maintenance costs, as these costs remain constant across different scheduling strategies. Secondly, the renewable energy utilization objective, represented by Eq. (18), aims to optimize the use of PV generation in order to mitigate the curtailment of solar energy. In fact, strictly pushing for absolute zero curtailment can sometimes be uneconomical. Lastly, the plant growth loss transforms the uncertainty in energy supply into uncertainty in the plant's growth environment in Eq. (19). These environmental fluctuations are then quantified as growth loss indices that reflect the deviation of actual growth conditions from the optimal range. The overall objective function f, which integrates these two aspects, is presented in Eq. (20).

$$C_{total} = C_{buy} + C_{sell} + C_{ES} \tag{14}$$

$$C_{buy} = \begin{cases} \int_0^T \left(\lambda_{buy}(t) \times P_{grid}(t)\right) dt, P_{grid}(t) > 0, \lambda_{buy}(t) > 0 \\ 0, P_{grid}(t) < 0 \end{cases} \tag{15}$$

$$C_{sell} = \begin{cases} 0, P_{grid}(t) > 0 \\ \int_0^T \left(\lambda_{sell}(t) \times P_{grid}(t)\right) dt, P_{grid}(t) < 0, \lambda_{sell}(t) > 0 \end{cases} \tag{16}$$

$$C_{ES} = \eta_{de} \times N_{cyc}(t) \times C_{battery} \tag{17}$$

$$\eta_{re} = \frac{\int_0^T \left(P_{pv}(t) - P_{pv \to ES}(t) \times \left(1 - \phi^2 \times \delta_{conv}^2\right)\right) dt}{\int_0^T P_{pv}(t) dt} \tag{18}$$

$$\Phi_{grow} = \int_0^T W_L \left(\frac{P_{supply} - P_{load}}{\left|\frac{\partial P_L}{\partial L}\right| \times L_{am}} \right)^2 + W_h \left(\frac{P_{supply} - P_{load}}{\left|\frac{\partial P_h}{\partial T_{in}}\right| \times T_{am}} \right)^2 + W_c \left(\frac{P_{supply} - P_{load}}{\left|\frac{\partial P_c}{\partial T_{in}}\right| \times T_{am}} \right)^2 dt \tag{19}$$

$$\min f = W_1 C_{total} - W_2 \eta_{re} + W_3 \Phi_{grow} \tag{20}$$

where W_1, W_2 and W_3 represent the weights of C_{total}, η_{re}, Φ_{grow}. W_L, W_h and W_c denote the weights associated with the environmental deviation. When $P_{grid}(t) > 0$, system purchases electricity from the power grid. When $P_{grid}(t) < 0$ indicates that power is being sold to the grid.

3.3. Constraint conditions

In the energy management of PV greenhouses, a set of constraints must be introduced to guarantee system reliability and operational stability. These constraints encompass energy balance, equipment hardware, and environmental conditions.

3.3.1. Energy balance

The energy balance constraints are formulated in Eqs. (21)–(22).

$$P_{pv \to load} + P_{ES \to load} + P_{grid \to load} = P_{load} \tag{21}$$

$$P_{pv \to load} + P_{pv \to ES} + P_{pv \to grid} = P_{pv} \tag{22}$$

3.3.2. Battery constraints

To ensure the safe operation of the battery system, the SOC and the battery power must be constrained within their upper and lower bounds, as formulated in Eqs. (23)–(24). The battery is constrained to prevent simultaneous charging and discharging, and discharging to power grid is prohibited when the PV power output is greater than zero in Eq. (25).

$$SOC_{min} \le SOC(t) \le SOC_{max} \tag{23}$$

$$P_{ES}^{min} \le P_{ES} \le P_{ES}^{max} \tag{24}$$

$$P_{ES}^{disch} \times P_{ES}^{charg} = 0, P_{pv} \times P_{ES \to grid}^{discharg} = 0 \tag{25}$$

where SOC_{min} and SOC_{max} is the lower and upper bounds of the SOC. P_{ES}^{min} and P_{ES}^{max} denote the lower and upper bounds of the battery power.

3.3.3. Power grid constraints

To ensure the feasibility and safety of power grid, the model considers active-reactive power balance, limits the exchanged power within the maximum interconnection capacity in Eqs. (26)–(28) [41]. To penalize unexpected power caused by forecasting errors, the real-time electricity price is set higher than the daily price in Eq. (29).

$$p_{j,t} - \sum_{i:ji \epsilon E} P_{ji,t} - \sum_{i:ij \epsilon E} P_{ji,t} = 0, \forall j \in N \tag{26}$$

$$q_{j,t} - \sum_{i:ji \epsilon E} Q_{ji,t} - \sum_{i:ij \epsilon E} Q_{ji,t} = 0, \forall j \in N \tag{27}$$

$$P_{grid}^{min} \le P_{grid} \le P_{grid}^{max} \tag{28}$$

$$\lambda_{buy}^{rt}(t) = (1 + \alpha)\lambda_{buy}(t) \tag{29}$$

where P_{grid}^{min} and P_{grid}^{max} is the lower and upper bounds of grid power. $\lambda_{buy}^{rt}(t)$ represents the real-time electricity price at time t.

3.3.4. Greenhouse constraints

To maintain a stable environment conducive to crop growth, the internal microclimate of the greenhouses must be controlled within appropriate ranges, as defined in Eqs. (30)–(33).

$$T_{min} \le T_{in}(t) \le T_{max} \tag{30}$$

$$H_{min} \le H_{in}(t) \le H_{max} \tag{31}$$

$$L_{min} \le L_{in}(t) \le L_{max} \tag{32}$$

$$CO_{min} \le CO_{in}(t) \le CO_{max} \tag{33}$$

where T_{min} and T_{max} respectively denote the lower and upper bounds of internal temperature. Similarly, H_{min} and H_{max} is the lower and upper bounds of internal humidity. L_{min} and L_{max} is the lower and upper bounds of internal light intensity. CO_{min} and CO_{max} is the lower and upper bounds of internal CO_2 concentration.

4. Quantum-enhanced energy management

4.1. Method structure

The proposed DAM-QLSTM-VQC method consists of two main stages: power forecasting and operational optimization, as shown in Fig. 2. In the forecasting stage, the DAM-QLSTM model is developed, which integrates quantum computing into the machine learning architecture, enabling effective modeling of both feature and temporal dependencies. This hybrid model effectively improves prediction accuracy. In the optimization stage, based on the prediction results, the VQC rolling optimization model is employed to solve complex non-convex optimization problem. This hybrid quantum-classical loop allows for efficient search of the solution in a high-dimensional decision space. By coupling DAM-QLSTM and VQC, the proposed method offers a coherent pipeline from forecasting to optimization, enabling more efficient of the PV greenhouses.

4.2. DAM-QLSTM forecasting model

4.2.1. Quantum-enhanced LSTM model

The LSTM, a variant of the Recurrent Neural Network (RNN), has been widely applied in renewable energy and load forecasting due to its ability to effectively mitigate the vanishing gradient problem commonly encountered in traditional RNN when dealing with time series prediction tasks. However, LSTM often suffer from computational bottlenecks and overfitting issues when processing high-dimensional and complex datasets. In recent years, the integration of quantum computing with LSTM has led to the development of QLSTM models, which leverage the parallelism and entanglement properties of quantum computing to improve the performance of LSTM in complex nonlinear dynamic forecasting tasks [42]. As illustrated in Fig. 3, the QLSTM model embeds quantum layers into each LSTM unit, significantly enhancing the model's capacity to handle complex and high-dimensional data.

The quantum state update within each LSTM cell follows specific principles of quantum mechanics. The update equations for the forget gate, memory gate, and output gate are provided in Eqs. (34)–(37),

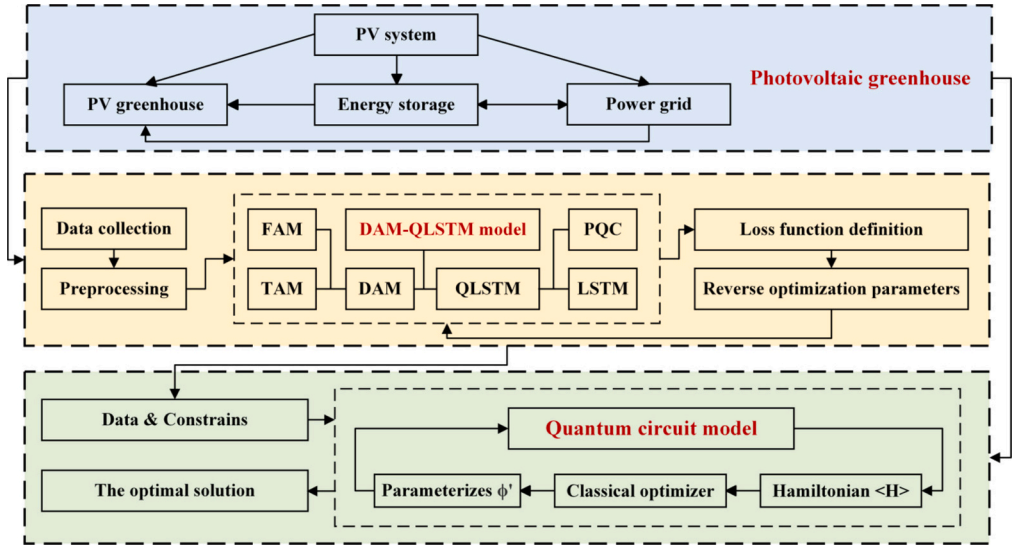


Fig. 2. The structure of DAM-QLSTM-VQC.

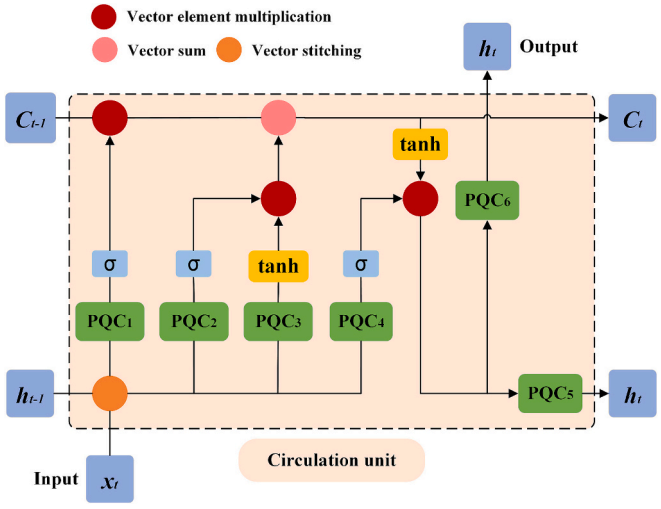


Fig. 3. The basic schematic diagram of QLSTM.

respectively. The incorporation of quantum-enhanced layers not only strengthens the model's ability to capture long-term dependencies in sequential data but also improves its adaptability to complex time series scenarios.

$$f_t = \sigma(PQC_1(X_t)) \tag{34}$$

$$i_t = \sigma(PQC_2(\vartheta_i)) \tag{35}$$

$$C_t = \sigma(PQC_1(X_t)) \times C_{t-1} + \sigma(PQC_2(X_t)) \times tanh(PQC_3(X_t)) \tag{36}$$

$$h_t = PQC_5(\sigma(PQC_4(X_t)) \times tanh(C_t)) \tag{37}$$

where X_t denotes the model input, i_t is the input gate, f_t represents the forget gate, C_t is the memory gate, and h_t corresponds to the output gate. *PQC* is the parametrized quantum circuit.

4.2.2. Dual attention mechanism

Considering the significant impact of environmental factors on both the supply and demand sides of energy systems, as well as the complexity arising from multi-variable and multi-constraint conditions, this study incorporates a DAM to enhance the predictive capability of the QLSTM. The DAM framework consists of the feature attention mechanism (FAM) and the multi-head temporal attention mechanism (MTAM), which together enable the model to effectively quantify the relevance between input variables and target outputs, while simultaneously reinforcing the influence of critical historical information on the forecasting outcomes [43].

In the first stage, the FAM assigns adaptive weights to multi-variate input features, such as PV generation parameters and environmental control variables, highlighting those most relevant to the prediction targets. To achieve this, FAM introduces a learnable weight vector that is optimized during the training process to maximize the model's sensitivity to critical features. Specifically, the FAM weight α_t is computed as shown in Eq. (38), where the use of a softmax function ensures that the sum of the attention weights is normalized to one.

$$\alpha_t = softmax\left[V_\alpha^T \cdot tanh(W_\alpha \bullet h_{t-1} + U_\alpha \bullet X_t + b_\alpha)\right] \tag{38}$$

where h_{t-1} represents the hidden state from the last time step, W_α and U_α are weight matrices, b_α is a bias vector, V_α^T is the scoring weight vector. *softmax* is an activation function.

In the second stage, the MTAM assigns dynamic weights to the model's historical hidden states. One head focuses on short-term temporal dependencies and the other on long-term dependencies. The attention weights are computed through residual connections and layer normalization. This module enables the model to not only capture features at the current time step but also leverage critical historical information to optimize the present prediction results. Specifically, the MTAM weight β_t is computed as described in Eqs. (39)–(40).

$$\beta_t^i = softmax\left[V_\beta^T \cdot tanh\left(W_\beta \times X_t + b_\beta\right)\right] \tag{39}$$

$$\beta_t = LayerNorm\left(X_t + Conat\left(\beta_t^1, \beta_t^2, \ldots\right)\right) \tag{40}$$

where β_t^i is the i-th head of temporal attention. W_β are weight matrices, b_β is a bias vector, V_β^T is the scoring weight vector.

4.2.3. DAM-QLSTM implementation

By integrating the quantum computing into the machine learning model, we construct the DAM-QLSTM model. Specifically, the training process of DAM-QLSTM involves the joint optimization of parameters within both the quantum-enhancement layer and the dual attention modules. This is achieved via a backpropagation algorithm that minimizes the prediction error, thereby enhancing the model's adaptability

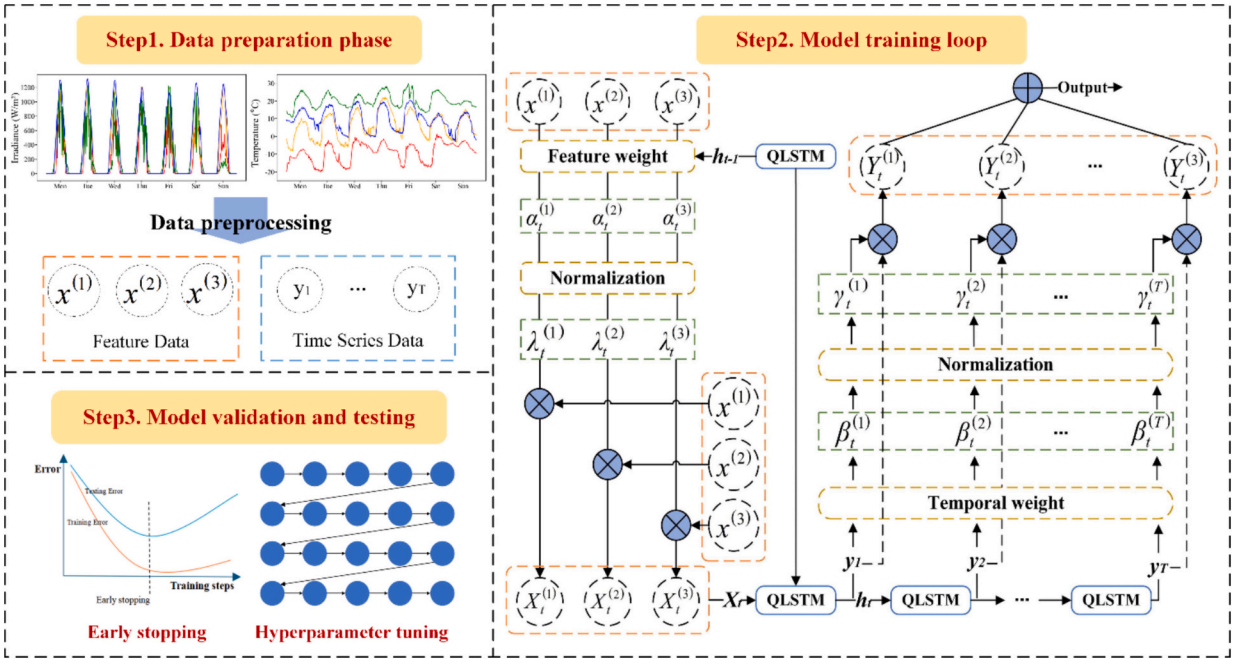


Fig. 4. The DAM-QLSTM forecasting model. The figure illustrates the PV power forecasting process, and the greenhouse load forecasting follows the same procedure.

to complex and dynamic environmental data. Fig. 4 illustrates the training workflow of the DAM-QLSTM model, encompassing data preprocessing, model training, validation, and testing stages.

During training, the FAM is responsible for identifying the most influential input features, while the MTAM highlights critical moments in the historical data that significantly impact prediction performance. To prevent overfitting and to maintain a balance between model complexity and generalization capability, the loss function combines the MSE with a regularization term, as defined in Eq. (41). By tuning the regularization coefficient, the model effectively manages the trade-off between capturing essential patterns and avoiding excessive complexity, ensuring both robustness and interpretability.

$$L = \frac{1}{N}\sum_{i=1}^{N}\left(P_i^{act} - P_i^{pre}\right)^2 + \lambda\left(\|\theta_\alpha\|^2 + \|\theta_\beta\|^2\right) \tag{41}$$

where L denotes the loss function, λ is the regularization coefficient, θ_α represents the parameter matrix of the FAM, θ_β denotes the parameter matrix of the MTAM. P_i^{act} denotes the actual value, P_i^{pre} represents the predicted value. N is the total number of data points.

Moreover, to further enhance the model's generalization capability, early stopping was employed during training to prevent overfitting, while cross-validation was utilized to evaluate the model's robustness. In terms of hyperparameter tuning, a grid search approach was adopted to optimize critical parameters such as learning rate, batch size, and the number of training epochs, ensuring that the DAM-QLSTM achieves consistent performance across diverse datasets. The prediction results provide reliable support for subsequent energy management decisions.

4.3. VQC-based rolling optimization model

4.3.1. Model framework

VQAs represent a hybrid quantum-classical algorithmic model that integrates classical optimization with quantum state evolution, as shown

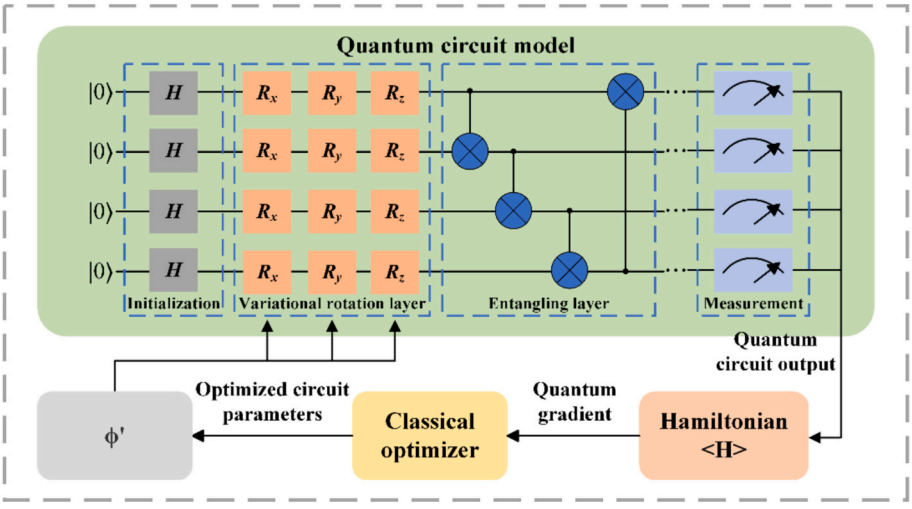


Fig. 5. The proposed VQC model. The quantum circuit adopted in this paper is displayed in the green box. (For interpretation of the references to colour in this figure legend, the reader is referred to the web version of this article.)

in Fig. 5. Compared to conventional methods, VQAs demonstrates superior parallel processing capabilities, offering significant efficiency advantages when tackling high-dimensional optimization problems [44]. VQAs is witnessing increasing application in the energy and power sector, particularly in areas such as power system operation and control [45], energy management [46], and distributed energy resource allocation [47].

In this paper, the VQC is employed as a rolling optimization model to optimize the energy allocation in the PV greenhouses system. The quantum circuit, which serves as the core of the VQC, consists of four components: initialization layer, variational rotation layer, entangling layer, and measurement layer, as illustrated in Fig. 5. Each quantum qubit represents an unknown variable in the optimization problem. The VQC constructs parameterized quantum states $|\varphi(\theta)\rangle$ through the parameterized quantum circuit, as shown in Eq. (42). Specifically, the process firstly initializes the quantum state$|\varphi_0\rangle$ using Hadamard gate. Secondly, we construct a parameterized quantum circuit using Hadamard gate, rotation gates such as R_x, R_y, R_z, along with entangling gates such as CNOT to generate the evolved quantum state $|\varphi(\theta)\rangle$. Lastly, we calculate the expectation value of the quantum state, updating the parameters iteratively, and using a classical optimizer until convergence to an approximate optimum is achieved.

$$|\varphi(\theta)\rangle = \left(\prod_{i=1}^{d}\left(R_X(\theta_1)R_Y(\theta_2)R_Z(\theta_3)\bullet\prod_{j=1}^{n-1}CNOT(j,j+1)\right)\right)|\varphi_0\rangle^{\otimes n} \tag{42}$$

where n represents the number of qubits. d is the circuit depth, where is set to 4.

4.3.2. VQC implementation

After constructing the VQC model, a complete optimization framework tailored to the PV greenhouses application is developed, consisting of data input, quantum state constructing, quantum optimization, and result. The proposed VQC optimization model comprises a data input module and a VQC optimization module in Fig. 6. Built upon a quantum-classical hybrid computing framework, this model enables optimization of multi-variable coupled systems, ensuring energy supply-demand balance while improving renewable energy utilization and reducing total operating cost.

For the data module, the system collects operational threshold parameters from various devices within the PV greenhouses, including PV panels, energy storage batteries, and agricultural machinery. These parameters not only serve as part of the model input but also define multi-variable coupling constraints in the optimization problem. In addition, predictive data such as PV generation and load demand serve as model inputs.

VQC leverages a redefined objective function described in Eqs. (43)–(46). In this paper, 7 qubits are employed to represent 7 unknown variables. A denormalization method is employed to map the expectation value of each qubit's Pauli-Z operator in the quantum circuit to the corresponding value of the unknown variable. Therefore, the objective function in this study can be reformulated as a new function with the circuit parameters θ as independent variables.

The quantum gradient is evaluated using the Parameter-Shift Rule, as shown in Eq. (47), which captures the nonlinear and entangled characteristics of quantum systems and enables exploration of high-dimensional, non-convex energy landscapes beyond the reach of classical methods. The circuit parameters are then optimized via the Adam optimizer, where the learning rate is set to 0.01 and the number of iterations to 5000.

$$\min f(x(\theta)) = W_1 C_{total}(x(\theta)) - W_2\eta_{re}(x(\theta)) + W_3\Phi_{grow}(x(\theta)) \tag{43}$$

$$x = 0.5\times(\mu(\theta)+1)\times(ub-lb)+lb \tag{44}$$

$$\mu(\theta) = [\langle Z_1\rangle, \langle Z_2\rangle, \langle Z_3\rangle \ldots, \langle Z_n\rangle]^T \tag{45}$$

$$\langle Z_n\rangle = \langle\varphi(\theta)|Z_n|\varphi(\theta)\rangle \tag{46}$$

$$\frac{\partial f}{\partial\theta} = \frac{f(\theta+\pi/2)-f(\theta-\pi/2)}{2} \tag{47}$$

where x is the unknown variables. θ is the circuit parameter.

This study embeds both the prediction results and the VQC optimization method into a rolling horizon model to effectively manage dynamic scheduling under uncertainties. The rolling horizon approach

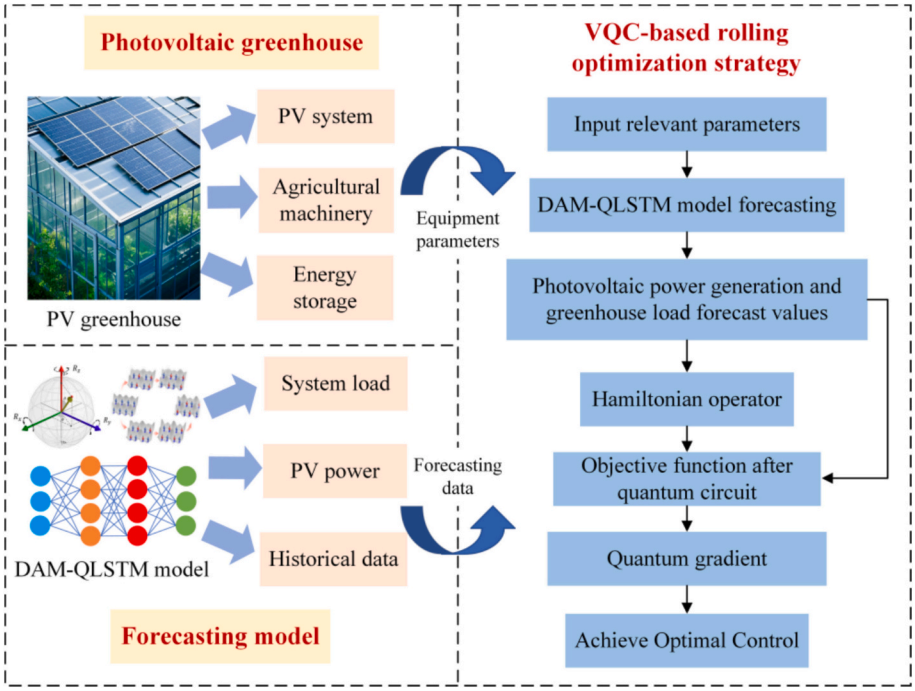


Fig. 6. The VQC rolling optimization model.

consists of iteratively solving the scheduling problem while advancing the optimization window at each decision point. In this formulation, the time discretization step is explicitly set to 15 min, allowing the model to accurately capture high-frequency fluctuations in energy dynamics. At each iteration, the VQC-based model evaluates a prediction horizon encompassing 4 look-ahead steps to determine the optimal operational schedule based on forecasted conditions. From this optimized sequence, only the decisions corresponding to the first-time step are implemented over a 15-min control horizon. The optimization window then rolls forward by one discrete step updating the initial system states and incorporating newly observed data for the subsequent iteration. The mathematical formulation of the objective function and the constraints, is comprehensively detailed in Sections 3.2 and 3.3.

5. Case study

5.1. Scenario description

This case study is conducted in a PV greenhouse located in Beijing, China, with geographic coordinates of 39.9042°N latitude and 116.4074°E longitude. The greenhouse covers a total area of 500 square meters, with dimensions of 25 m in length, 20 m in width, and 15 m in height, as shown in Fig. 7. The energy storage system employed in the greenhouse consists of lithium-ion batteries with a total capacity of 10 kWh. PV panels are installed on the rooftop, covering 30% of the roof surface and providing an installed capacity of 25 kW. Because this study primarily investigates the short-term energy management of existing PV greenhouses, the capacities of the PV arrays and batteries are treated as predetermined. However, the optimal capacity sizing of such systems remains a vital avenue for future research.

The greenhouse maintains a stable internal temperature between 24 °C and 26 °C and utilizes supplemental lighting at night to support crop growth. Environmental data, including meteorological conditions, PV generation, and load demand, are collected at 15-min intervals.

5.2. Parameter setting

To ensure the fairness, reliability, and reproducibility of the comparison, all models are trained and tested under a consistent computational environment. Specifically, classical computations are executed on a laptop equipped with an AMD Ryzen 54,500 U CPU @ 2.4 GHz and 8 GB RAM, while quantum computations are performed on the Origin Wukong quantum computing platform. During the training phase, classical optimization is performed using the Adam optimizer with an initial learning rate of 0.01. Each model is trained for 40 epochs with a batch size of 1.

Moreover, the energy storage system is primarily used to mitigate supply-demand imbalances during PV generation fluctuations or load demand peaks. The key specifications of the energy storage system are summarized in Table 2.



Fig. 7. The PV greenhouse photo in this study.

Table 2
Parameters of the energy storage system.

Parameters	Values	Parameters	Values
C_0	10 KWh	SOC_{inital}	50%
ϕ^{disch}, ϕ^{charg}	95%	δ_{conv}	90%
SOC_{min}	20%	P_{SE}^{max}	20
SOC_{max}	80%	P_{SE}^{min}	0

The power grid serves as a backup energy source, supplying additional electricity during periods of PV power deficiency or peak load demand. In this study, the electricity pricing scheme adopted in Beijing is considered, comprising three pricing tiers: peak, flat, and valley. Specifically, the peak tariff is set at $0.23/kWh (from 10:00 to 13:00 and 17:00 to 22:00), the flat tariff at $0.14/kWh (from 7:00 to 10:00, 13:00 to 17:00, and 22:00 to 23:00), and the valley tariff at $0.05/kWh (from 23:00 to 07:00 the next day). During periods of PV overproduction, sale electricity can be fed back into the grid at the feed-in Beijing tariff of $0.05/kWh, as shown in Extended Fig. 1.

5.3. Data information

All models are trained on a unified dataset to ensure consistency and comparability of results. The dataset originates from the operational records of PV greenhouse within the smart park operated by Beijing University of Agriculture.

The dataset comprises representative daily data from a PV greenhouse, collected during the first week of January, April, July, and October, thereby capturing seasonal variations across winter, spring, summer, and autumn. Input features include solar irradiance, ambient temperature, and humidity, recorded at a 15-min temporal resolution, as illustrated in Fig. 8. In January, PV power generation ranges from 49.38 kWh to 100.40 kWh, primarily limited by reduced daylight hours and low solar irradiance. By April, output increases substantially to 108.94–182.63 kWh due to enhanced solar exposure. In July, the rainy season in Beijing introduces significant variability, with generation fluctuating between 20.20 and 125.82 kWh. As precipitation decreases in October, the output stabilizes within the range of 131.00–159.69 kWh.

The dataset is partitioned into training, validation, and test sets with a ratio of 5:1:1. Prior to model training, all input features are standardized to zero mean and unit variance to mitigate the impact of scale heterogeneity and enhance training stability.

5.4. Feature relationship analysis

The Pearson correlation coefficient heat map, as shown in Fig. 9, illustrates the linear relationships between PV power and 7 meteorological variables [48]. The results reveal that PV power exhibits a remarkably strong positive correlation with direct and diffuse radiation, where the correlation coefficient reaches 0.983 and 0.759. This indicates that the magnitude of solar irradiance plays an almost linear and decisive role in determining the power output of PV systems. Such a relationship arises from the inherent dependency of PV modules on solar radiation, particularly the direct component, which is more efficiently converted into electrical energy by PV cells. Wind speed also maintains a moderately positive correlation with PV power, which can likely be attributed to the role of wind in lowering module temperature and potentially reducing cloud cover, both of which contribute to enhanced energy conversion efficiency.

By contrast, the correlation between ambient temperature and PV power is comparatively weak. This supports that higher temperatures tend to reduce the performance of PV modules, although an increase in

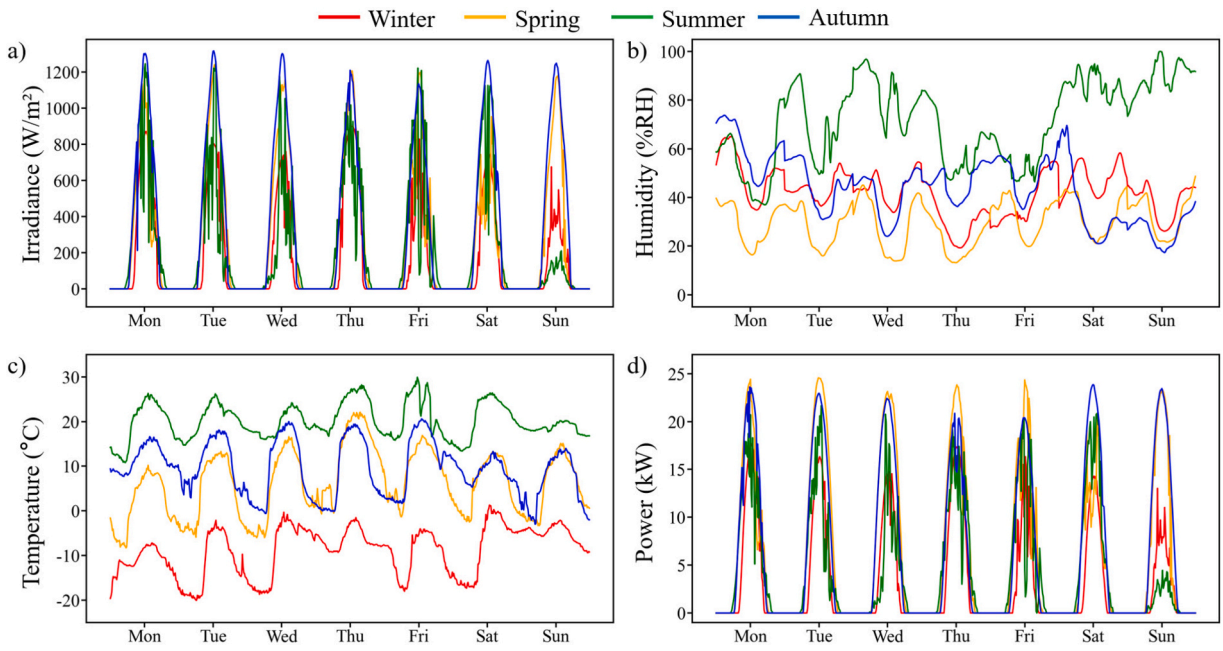


Fig. 8. Typical day data from the PV greenhouse: (a) solar irradiance, (b) humidity, (c) temperature, and (d) PV output power. The dataset originates from the operational records of the PV greenhouse within the smart park operated by Beijing University of Agriculture.

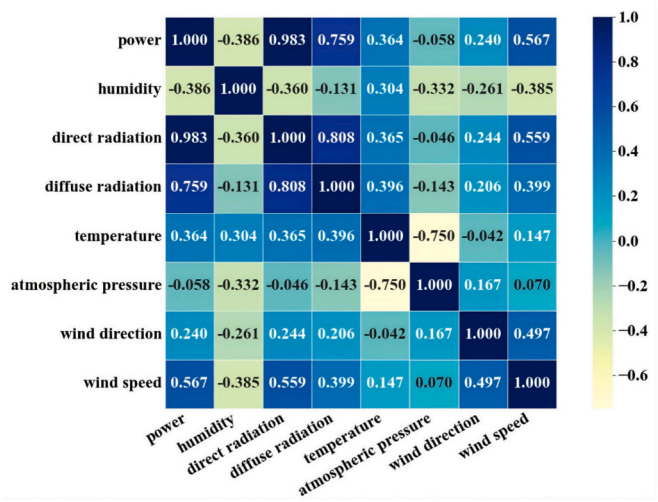


Fig. 9. The pearson correlation coefficient heat map.

temperature often coincides with elevated solar radiation. In addition, a moderate negative correlation is found between humidity and PV power output, implying that high humidity levels may suppress power generation, most likely by reducing radiation transmittance or by contributing to greater cloud coverage.

Furthermore, both wind direction and atmospheric pressure exhibit only minimal correlation with PV output. Overall, the findings indicate that direct radiation, diffuse radiation, and wind speed serve as the primary meteorological drivers of PV performance, while temperature and humidity act as secondary factors that influence energy conversion under varying environmental conditions.

5.5. Performance evaluation of forecasting models

In this section, various error metrics used for performance evaluation include Mean Squared Error (MSE), Root Mean Squared Error (RMSE), and Mean Absolute Error (MAE) [49]. MSE measures the average of squared differences between predicted and actual values. RMSE evaluates the typical magnitude of prediction errors. MAE evaluates the robustness of predictions by computing the average absolute differences The formulas are presented in Eqs. (48)–(50).

$$MSE = \frac{1}{N}\sum_{i=1}^{N}\left(P_i^{act} - P_i^{pre}\right)^2 \tag{48}$$

$$RMSE = \sqrt{\frac{1}{N}\sum_{i=1}^{N}\left(P_i^{act} - P_i^{pre}\right)^2} \tag{49}$$

$$MAE = \frac{1}{N}\sum_{i=1}^{N}\left|P_i^{act} - P_i^{pre}\right| \tag{50}$$

where $P_{PV}^{pre}(t)$ denotes the predicted PV generation power, $P_{demand}^{pre}(t)$ represents the predicted load demand. N is the total amount of data.

5.6. Comparison of prediction results

To validate the effectiveness of the proposed DAM-QLSTM model for power forecasting, a comparative analysis is conducted with fore representative baseline models: DAM-LSTM, Attention-LSTM, QLSTM, and LSTM. DAM-LSTM reflects the role of the dual attention mechanism, QLSTM reflects the impact of the quantum-enhanced structure. Attention-LSTM and LSTM serve as the standard baseline.

Fig. 10 presents a comparison between the actual PV power generation and the predicted values from different models. The results demonstrate that the DAM-QLSTM model exhibits superior stability, particularly during periods of intense PV power fluctuations. It consistently yields lower prediction errors compared to other models, highlighting its advantage in modeling complex time-series data with high robustness. In contrast, other models show larger prediction deviations during PV power peaks and periods of high greenhouse energy demand. This is especially evident in the traditional LSTM model, which struggles to accurately capture the complex multivariable coupling relationships inherent in the PV greenhouse system. These findings suggest that the quantum computation contribute to more efficient extraction and representation of nonlinear features and high-order correlations among

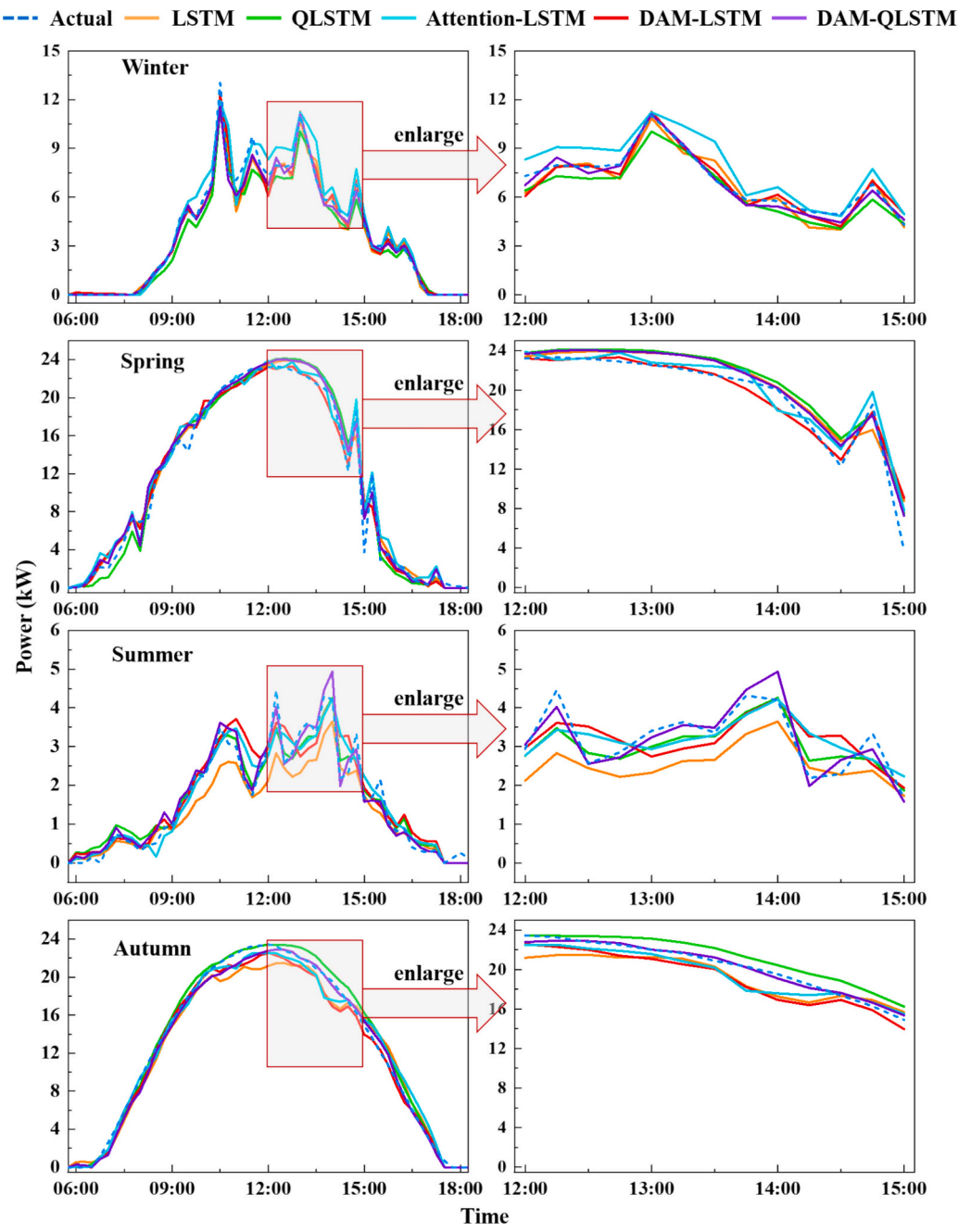


Fig. 10. Comparison of predicted and actual PV power across five models in one day from each season. The inset on the right provides an enlarged view of the prediction results within the box, showing that the proposed model exhibits the smallest deviation between the predicted and actual curves. The time resolution is 15 min.

Table 3
Forecasting errors of five models in one day during four seasons.

	Winter			Spring			Summer			Autumn		
	MSE	RMSE	MAE	MSE	RMSE	MAE	MSE	RMSE	MAE	MSE	RMSE	MAE
LSTM	0.2522	0.5022	0.2531	0.8811	0.9387	0.4534	0.1395	0.3735	0.188	0.8408	0.917	0.5586
QLSTM	0.2176	0.4665	0.2149	0.7785	0.8823	0.4593	0.0457	0.2138	0.1231	0.4086	0.6293	0.2932
Attention-LSTM	0.1479	0.3846	0.1718	0.7752	0.8804	0.3979	0.1156	0.3401	0.1761	0.3904	0.6249	0.3209
DAM-LSTM	0.1186	0.3444	0.1822	0.7515	0.8669	0.4459	0.1132	0.3365	0.178	0.4296	0.6554	0.3635
DAM-QLSTM	0.0908	0.3013	0.1361	0.6705	0.8188	0.4036	0.0227	0.1664	0.0936	0.2195	0.4685	0.2645

variables, thereby enhancing predictive performance.

To quantitatively evaluate the prediction accuracy, MSE, RMSE, and MAE are calculated for each model on the test set, as summarized in Table 3. Compared to the LSTM model, the DAM-QLSTM model reduces MSE, RMSE, and MAE by 52.5%, 35.7%, and 38.2%, respectively. Moreover, DAM-QLSTM consistently outperforms DAM-LSTM and QLSTM across all evaluation metrics, demonstrating its superior accuracy and generalization capability. In summary, DAM-QLSTM shows significantly better performance in PV power forecasting, providing a more accurate data foundation for subsequent optimization and scheduling using the VQC model.

5.7. Comparison of optimization results

Based on the above prediction results of DAM-QLSTM, this study compares the VQC model with three representative optimization algorithms: PSO, quantum particle swarm optimization (QPSO) and MPC, to validate the effectiveness of the proposed operational optimization strategy. PSO is as a widely used classical heuristic baseline. QPSO represents a typical quantum heuristic optimization algorithm. MPC is a robust classical method. These models are applied to the energy management of the PV greenhouse across all four seasons. Fig. 11 illustrates the energy scheduling results of VQC. The energy scheduling results of PSO, QPSO and MPC are shown in extended Fig. 2–4. As shown, the VQC model allocates more PV generation for self-consumption, significantly improving the renewable energy utilization ratio within the greenhouse system.

Table 4 presents the quantitative results for renewable energy utilization and total operational costs under each model, further confirming the overall superiority of the VQC model. The VQC model consistently achieves the lowest total operating cost. On average, VQC model increases renewable energy utilization by 9.6% and reduces total operational costs by 15.4% compared to PSO. When compared with QPSO, VQC achieves an 6.3% improvement in renewable energy utilization and a 9.9% reduction in cost. Compared with MPC, VQC can reduce 1.5% in cost. The utilization ratio of VQC does not reach a full 100% primarily because a portion of the scheduled energy is directed into the battery storage system. Due to inherent charging-discharging efficiency losses, part of the stored energy cannot be fully recovered, preventing absolute utilization.

Despite its simplicity, PSO is prone to premature convergence and getting trapped in local optima. In contrast, QPSO incorporates quantum mechanisms to enhance search capabilities. However, its particles tend to converge toward the mean of all personal best positions, limiting its ability to identify optimal solutions located near the boundaries of the feasible region. This characteristic results in higher total operating cost and lower renewable energy utilization for QPSO. Moreover, short-term dispatch using MPC generates myopic decisions, trapping the system in local optima by greedily dispatching PV generation directly to the load or grid to minimize immediate cost and maximize utilization. VQC leverages quantum computation for enhanced exploration while relying on classical optimization for improved stability and convergence, which enables VQC to simultaneously obtain better results.

Fig. 12 illustrates the daily power consumption from the grid to the PV greenhouse across four seasons. It is evident that the VQC model results in the lowest grid electricity consumption. The reduced reliance on electricity purchased from the grid can be attributed to the VQC model that enhances the ability to utilize PV energy, as it prioritizes meeting greenhouse energy load and storing excess generation in batteries, instead of prematurely feeding renewable energy electricity back into the grid. As a result, the VQC model has significantly reduced the reliance on grid electricity.

In addition to electricity costs, grid-sourced energy entails CO_2, SO_2, and NO_x emissions [44]. The environmental impacts of different strategies are summarized in Table 5. Benefiting from more efficient PV utilization, the VQC model achieves the lowest emissions across all pollutants. Compared to the PSO model, VQC reduces CO_2 and pollutant emissions by 9.9%. Relative to QPSO and MPC, CO_2 and pollutant emissions are lowered by 9.1% and 4.7%, respectively.

To evaluate the impact of forecasting uncertainty on subsequent energy scheduling decisions, we performed a comparative study using the PV power predictions generated by four models based on a winter

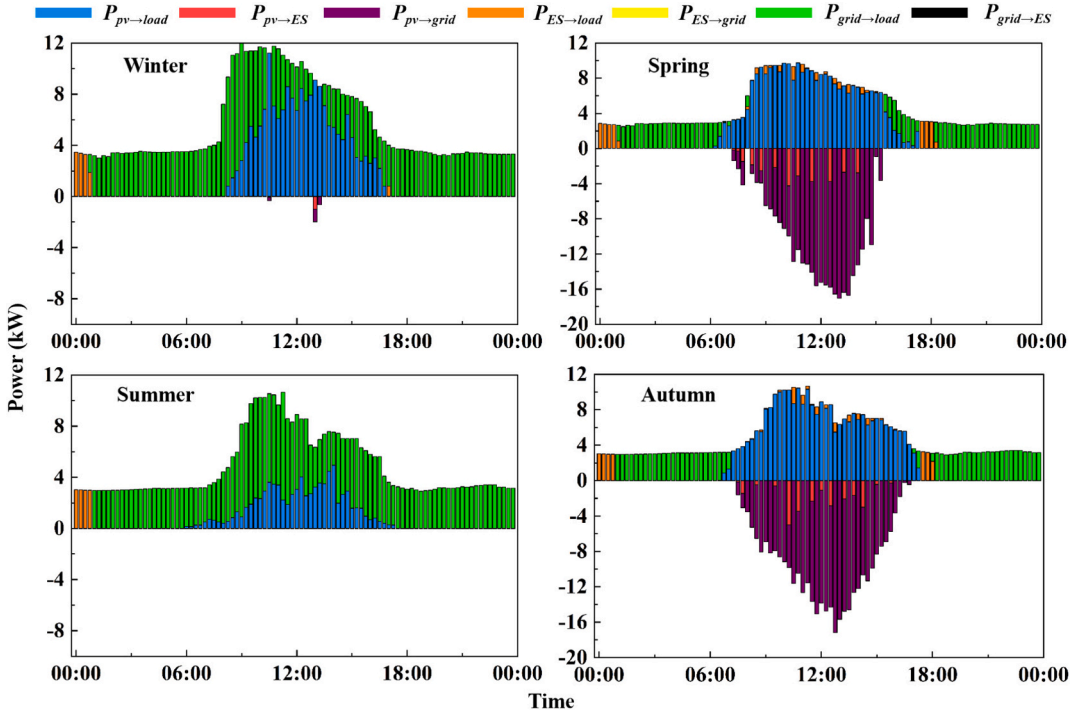


Fig. 11. Energy scheduling results of DAM-QLSTM-VQC model in one day from each season. The upper part of the y-axis represents the energy flow directed to the greenhouse, while the lower part indicates the energy flow toward energy storage system and power grid. The time resolution is 15 min.

Table 4
Performance comparison of PSO, QPSO, MPC and VQC models in terms of cost, renewable energy utilization ratio and plant growth loss in one day from each season based on the result of DAM-QLSTM.

	Winter			Spring			Summer			Autumn		
	C_{total} ($)	η_{re} (%)	Φ_{grow}	C_{total} ($)	η_{re} (%)	Φ_{grow}	C_{total} ($)	η_{re} (%)	Φ_{grow}	C_{total} ($)	η_{re} (%)	Φ_{grow}
PSO	13.91	89.49	0.00	2.23	90.13	0.00	15.36	91.17	0.00	1.96	90.59	0.00
QPSO	13.39	92.48	0.00	1.70	92.94	0.00	15.00	92.85	0.00	1.31	93.53	0.00
MPC	12.59	100.00	0.00	1.37	100.00	0.00	14.41	100.00	0.00	0.86	100.00	0.00
VQC	12.56	99.70	0.00	0.87	98.70	0.00	14.38	99.40	0.00	0.43	98.90	0.00

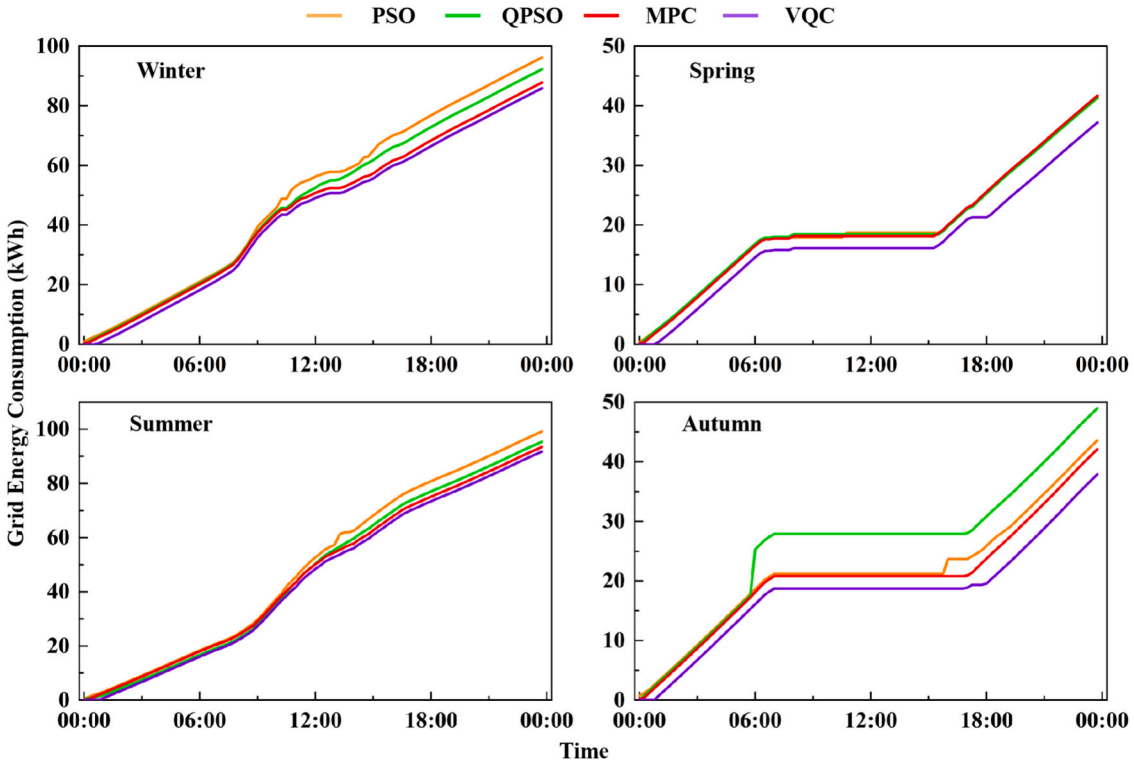


Fig. 12. Grid energy consumption under four models in one day from each season. The curves show the variation of the energy consumption of the power grid over time under different models. The time resolution is 15 min.

Table 5
CO_2 and pollutant emissions under four models in one day from each season. For each kWh of electricity purchased from the grid, some pollutants are produced.

	Winter			Spring		Summer			Autumn			
	CO_2 (kg)	SO_2 (kg)	NO_x (kg)	CO_2 (kg)	SO_2 (kg)	NO_x (kg)	CO_2 (kg)	SO_2 (kg)	NO_x (kg)	CO_2 (kg)	SO_2 (kg)	NO_x (kg)
PSO	108.74	0.92	0.27	46.93	0.40	0.12	112.05	0.95	0.28	49.28	0.42	0.12
QPSO	104.28	0.89	0.26	46.71	0.40	0.12	107.80	0.92	0.27	55.35	0.47	0.14
MPC	99.22	0.84	0.25	47.13	0.40	0.12	105.62	0.90	0.26	47.58	0.40	0.12
VQC	97.06	0.83	0.24	42.05	0.36	0.11	103.69	0.88	0.26	42.83	0.36	0.11

day described in Section 5.5. These predicted values were then used as inputs to the VQC-based rolling optimization model. The resulting PV power dispatch decisions are illustrated in Fig. 13. The results reveal that LSTM and QLSTM tend to systematically under-estimate PV output. Consequently, a portion of the available solar energy remains unused, increasing total operating cost. In contrast, DAM-LSTM frequently over-estimates PV generation, causing the optimization model to allocate energy assuming more renewable availability than actually exists. When real-time generation falls short, the system must purchase additional peak-price electricity from the grid, leading to greater cost escalation and inefficient energy allocation. By comparison, DAM-QLSTM demonstrates the most accurate forecasting performance, enabling more reliable scheduling, and minimized total operating cost. In addition, while we account for generation and load uncertainties through power forecasting, other sources of uncertainty such as price volatility and equipment failure may further affect system performance. Conducting research on the impact of other sources of uncertainty in future study is of significant importance.

Table 6 summarizes the quantitative comparison results. The data show that the DAM-QLSTM-VQC model achieves the lowest total operating cost of $12.56, representing a 4.05% reduction compared with the baseline LSTM-VQC model. Furthermore, the DAM-QLSTM-VQC model attains a renewable energy utilization ratio of over 99%.

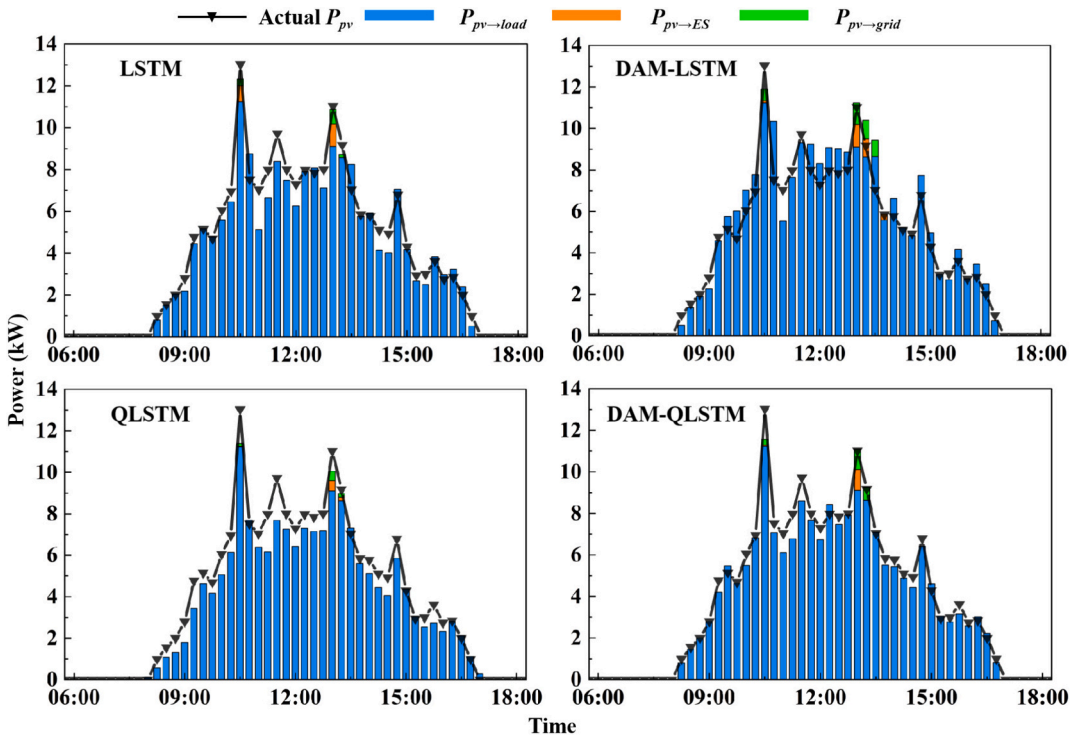


Fig. 13. PV power scheduling results of LSTM-VQC, QLSTM-VQC, DAM-LSTM-VQC, DAM-QLSTM-VQC models in one winter day described in Section 5.5. LSTM and QLSTM tend to under-estimate PV output, resulting in the inability to fully utilize PV power. DAM-LSTM over-estimates PV output, leading to must purchase additional peak-price electricity from the grid. DAM-QLSTM model is the most accurate.

Table 6
Performance comparison of four models in terms of cost, renewable energy utilization ratio and plant growth loss in one winter day described in Section 5.5.

	C_{total} ($)	η_{re} (%)	Φ_{grow}
LSTM-VQC	13.09	99.21	0.00
QLSTM-VQC	13.26	99.59	0.00
DAM-LSTM-VQC	13.47	99.33	0.00
DAM-QLSTM-VQC	12.56	99.70	0.00

5.8. Discussion

Although the proposed model demonstrates promising results in integrating quantum computing into energy management, several intrinsic limitations remain.

First, the parameterized quantum circuit may suffer from barren plateaus, where gradients vanish as circuit depth increases, hindering effective optimization. This issue is mitigated in our design by adopting a relatively shallow circuit (4 layers) and a narrow parameter initialization range $(-0.1, 0.1)$, yet the risk cannot be entirely eliminated.

Second, due to the immaturity of quantum hardware, the practical applicability of the proposed framework in actual energy systems remains to be systematically validated. Noise, limited qubit counts, short coherence times, and restricted connectivity may significantly degrade the performance of circuits that perform well in simulations.

Third, the adopted model may not completely consider the operational uncertainties and strict physical constraints present in real energy systems. Factors such as equipment degradation, response delays, and network security limits may influence model performance.

In future work, we plan to further explore the integration of quantum computing with energy storage systems to enhance the overall operational efficiency of energy systems. As quantum hardware continues to advance, its application in more complex energy systems is expected to offer innovative solutions to emerging challenges in energy management.

Additionally, the challenges addressed in this study are not exclusive to PV greenhouses. Similar characteristics arise in a range of energy management systems featuring strong coupling and inherent uncertainty. In this context, the proposed method may also be applicable to scenarios such as PV buildings and distributed renewable energy charging stations. Globally, off-grid PV greenhouses will have extensive application scenarios in underdeveloped regions, where the absence of grid support increases reliance on energy storage. In such cases, seasonal energy storage like hydrogen may offer potential solutions, but their practical feasibility requires further investigation. These observations point to several promising directions for future work.

6. Conclusion

This paper proposes a DAM-QLSTM-VQC method to address the energy management challenges in the PV greenhouses: the uncertainty of energy supply and demand as well as the complexity of coordinated optimization. The main contributions are summarized as follows:

(1) A DAM-QLSTM forecasting model is developed, which integrates quantum computing into the machine learning architecture, enabling effective modeling of both feature and temporal dependencies. The model exploits quantum entanglement characteristic, capturing the nonlinear and dynamic coupling within the input dataset, significantly improving forecasting accuracy. Compared to the conventional LSTM model, the DAM-QLSTM reduces MSE, RMSE, and MAE by 52.5%, 35.7%, and 38.2%.
(2) A VQC rolling optimization model is developed to solve the complex non-convex optimization problem in the PV greenhouses, which adopts quantum gradients to efficiently update parameters. In experiments, the VQC model achieves over 99% renewable energy utilization, a total operating cost of $ 28.29, and 285.63 kg of carbon emissions. Compared with PSO, it improves renewable energy utilization by 9.6%, respectively reduces total operating cost, carbon and pollutant emissions by

15.4%, 9.9%. Compared with MPC, it decreases cost by 1.5% and emissions by 4.7%, but reduces utilization by 1.0%.

(3) The proposed method is validated using practical data from a representative PV greenhouse in Beijing. Simulation results confirm that the DAM-QLSTM-VQC method improves system efficiency, outperforms traditional forecasting and optimization approach in terms of both accuracy and robustness. This study verifies quantum computing in practical energy management and opens new directions for integrating quantum technology into smart agricultural system.

Compliance with ethics guidelines

Zhenhao Weng, Zhanpeng Xu, Ruichong Li, Longze Wang, Zhehan Li, Yan Zhang and Meicheng Li declare that they have no conflict of interest or financial conflicts to disclose.

CRediT authorship contribution statement

Zhenhao Weng: Writing – review & editing, Writing – original draft, Software, Project administration, Methodology, Investigation, Data curation, Conceptualization. **Zhanpeng Xu:** Writing – review & editing, Investigation. **Ruichong Li:** Writing – review & editing, Investigation. **Longze Wang:** Writing – original draft, Methodology, Investigation, Funding acquisition. **Zhehan Li:** Writing – review & editing. **Yan Zhang:** Funding acquisition, Formal analysis. **Meicheng Li:** Writing – review & editing, Validation, Supervision, Resources, Project administration, Methodology, Investigation, Funding acquisition, Conceptualization.

Declaration of competing interest

The authors declare that they have no known competing financial interests or personal relationships that could have appeared to influence the work reported in this paper.

Acknowledgments

This work is supported partially by National Natural Science Foundation of China (Grant Nos. 71974055), 2022 Strategic Research Key Project of Science and Technology Commission of the Ministry of Education, Beijing Science and Technology Project (Z211100004621010), the project of China Three Gorges Corporation named key technologies of intelligent joint regulation and operation with grid connected friendly in power station group of wind, solar photovoltaic and energy storage (WWKY-2021-0173), Huaneng Group Headquarters Science and Technology Project (HNKJ20-H88), State Key Laboratory of Alternate Electrical Power System with Renewable Energy Sources (Grant No. LAPS25002), Fundamental Research Funds for the Central Universities (2025MS048) and the NCEPU “Double First-Class” Program.

Appendix A. Supplementary data

Supplementary data to this article can be found online at https://doi.org/10.1016/j.apenergy.2026.128142.

Data availability

Data will be made available on request.

References

[1] Tigchelaar M, Battisti D, Naylor R, et al. Future warming increases probability of globally synchronized maize production shocks. Proc Natl Acad Sci USA 2018;115(26):6644–9. https://doi.org/10.1073/pnas.1718031115.

[2] Zhang L, Liu D, Cai G, et al. An optimal dispatch model for virtual power plant that incorporates carbon trading and green certificate trading. Int J Electr Power Energy Syst 2023;144:108558. https://doi.org/10.1016/j.ijepes.2022.108558.

[3] Wang L, Mao Y, Li Z, et al. Life cycle carbon emission intensity assessment for photovoltaic greenhouses: a case study of Beijing City, China. Renew Energy 2024;230:120775. https://doi.org/10.1016/j.renene.2024.120775.

[4] Lin D, Dong Y, Ren Z, et al. Hierarchical optimization for the energy management of a greenhouses integrated with grid-tied photovoltaic–battery systems. Appl Energy 2024;374:124006. https://doi.org/10.1016/j.apenergy.2024.124006.

[5] Chen W, You F. Energy optimization of bitcoin mining integrated greenhouse with model predictive control. Appl Energy 2025;395:126256. https://doi.org/10.1016/j.apenergy.2025.126256.

[6] Parajuli S, Bhattarai TN, Gorjian S, et al. Assessment of potential renewable energy alternatives for a typical greenhouse aquaponics in Himalayan Region of Nepal. Appl Energy 2023;344:121270. https://doi.org/10.1016/j.apenergy.2023.121270.

[7] Gao Y, Dong J, Isabella O, et al. Modeling and analyses of energy performances of photovoltaic greenhouses with sun-tracking functionality. Appl Energy 2019;233:424–42. https://doi.org/10.1016/j.apenergy.2018.10.019.

[8] Morstyn T, Wang X. Opportunities for quantum computing within net-zero power system optimization. Joule 2024;8(6):1619–40. https://doi.org/10.1016/j.joule.2024.03.020.

[9] Mastroianni C, Plastina F, Scarcello L, et al. Assessing quantum computing performance for energy optimization in a prosumer community. IEEE Trans Smart Grid 2024;15(1):444–56. https://doi.org/10.1109/TSG.2023.3286106.

[10] Nikmehr N, Zhang P, Zheng H, et al. Quantum annealing-infused microgrids formation: distribution system restoration and resilience enhancement. IEEE Trans Power Syst 2025;40(1):463–75. https://doi.org/10.1109/TPWRS.2024.3399122.

[11] Jiang Y, Liang Z, Li Y, et al. Optimal PMU placement via quantum optimization. IEEE Trans Smart Grid 2025;16(4):3125–41. https://doi.org/10.1109/TSG.2025.3564889.

[12] Cerezo M, Arrasmith A, Babbush R, et al. Variational quantum algorithms. Nat Rev Phys 2021;3:625–44. https://doi.org/10.1038/s42254–021–00348-9.

[13] Hartmann C, Zhang J, Calaza C, et al. Quantum annealing based power grid partitioning for parallel simulation. IEEE Trans Power Syst 2025;40(6):4958–70. https://doi.org/10.1109/TPWRS.2025.3578243.

[14] Ajagekar A, You F. Variational quantum circuit based demand response in buildings leveraging a hybrid quantum-classical strategy. Appl Energy 2024;364:123244. https://doi.org/10.1016/j.apenergy.2024.123244.

[15] Silva F, Carvalho P, Ferreira L, et al. A QUBO formulation for minimum loss network reconfiguration. IEEE Trans Power Syst 2023;38(5):4559–71. https://doi.org/10.1109/TPWRS.2022.3214477.

[16] Dai S. Optimal energy management of multi-energy multi-microgrid networks using mountain gazelle optimizer for cost and emission reduction. Energy 2025;329:136640. https://doi.org/10.1016/j.energy.2025.136640.

[17] Zhang K, Yu J, Ren Y. Demand side management of energy consumption in a photovoltaic integrated greenhouse. Int J Electr Power Energy Syst 2022;134:107433. https://doi.org/10.1016/j.ijepes.2021.107433.

[18] Zhu Y, Li G, Jiang Y, et al. Predicting photovoltaic greenhouses irradiance at low-latitudes of plateau based on ultra-short-term time series. Renew Energy 2025;239:122053. https://doi.org/10.1016/j.renene.2024.122053.

[19] Pinto G, Deltetto D, Capozzoli A. Data-driven district energy management with surrogate models and deep reinforcement learning. Appl Energy 2021;304:117642. https://doi.org/10.1016/j.apenergy.2021.117642.

[20] Zhu Y, Li M, Ma X, et al. Solar irradiance prediction with variable time lengths and multi-parameters in full climate conditions based on photovoltaic greenhouse. Energy Convers Manag 2024;315:118758. https://doi.org/10.1016/j.enconman.2024.118758.

[21] Hu G, You F. Renewable energy-powered semi-closed greenhouses for sustainable crop production using model predictive control and machine learning for energy management. Renew Sust Energ Rev 2022;168:112790. https://doi.org/10.1016/j.rser.2022.112790.

[22] Ajagekar A, Decardi-Nelson B, You F. Energy management for demand response in networked greenhouses with multi-agent deep reinforcement learning. Appl Energy 2024;355:122349. https://doi.org/10.1016/j.apenergy.2023.122349.

[23] Zhao Z, Lee C, Ren J. A two-level charging scheduling method for public electric vehicle charging stations considering heterogeneous demand and nonlinear charging profile. Appl Energy 2024;355:122278. https://doi.org/10.1016/j.apenergy.2023.122278.

[24] Xu H, Zhang A, Wang Q, et al. Quantum reinforcement learning for real-time optimization in electric vehicle charging systems. Appl Energy 2025;383:125279. https://doi.org/10.1016/j.apenergy.2025.125279.

[25] Gao F, Wu G, Guo S, et al. Solving DC power flow problems using quantum and hybrid algorithms. Appl Soft Comput 2023;137:110147. https://doi.org/10.1016/j.asoc.2023.110147.

[26] Nikmehr N, Zhang P, Bragin M. Quantum distributed unit commitment: an application in microgrids. IEEE Trans Power Syst 2022;37(5):3592–603. https://doi.org/10.1109/TPWRS.2022.3141794.

[27] Hong Y, Rioflorido C, Zhang W. Hybrid deep learning and quantum-inspired neural network for day-ahead spatiotemporal wind speed forecasting. Expert Syst Appl 2023;241:122645. https://doi.org/10.1016/j.eswa.2023.122645.

[28] Bi Z, Yang X, Wang B, et al. Quantum annealing algorithm for fault section location in distribution networks. Appl Soft Comput 2023;149(A):110973. https://doi.org/10.1016/j.asoc.2023.110973.

[29] Feng F, Zhou Y, Zhang P. Quantum power flow. IEEE Trans Power Syst 2021;36(4):3810–2. https://doi.org/10.1109/TPWRS.2021.3077382.

[30] Feng F, Zhang P, Bragin M, et al. Novel resolution of unit commitment problems through quantum surrogate lagrangian relaxation. IEEE Trans Power Syst 2022;38(3):2460–71. https://doi.org/10.1109/TPWRS.2022.3181221.
[31] Li J, Zhou T, Keke H, et al. Distributed quantum multiagent deep meta reinforcement learning for area autonomy energy management of a multiarea microgrid. Appl Energy 2023;343:121181. https://doi.org/10.1016/j.apenergy.2023.121181.
[32] Biamonte J, Wittek P, Pancotti N, et al. Quantum machine learning. Nature 2017;549:195–202. https://doi.org/10.1038/nature23474.
[33] Song W, Cattani C, Chi C. Multifractional brownian motion and quantum-behaved particle swarm optimization for short term power load forecasting: an integrated approach. Energy 2019;194:116847. https://doi.org/10.1016/j.energy.2019.116847.
[34] Chinzei K, Yamano S, Tran Q, et al. Trade-off between gradient measurement efficiency and expressivity in deep quantum neural networks. npj Quantum Inf 2025;11:79. https://doi.org/10.1038/s41534–025–01036-7.
[35] Ravishankar E, Booth R, Saravitz C, et al. Achieving net zero energy greenhouses by integrating semitransparent organic solar cells. Joule 2019;4(2):490–506. https://doi.org/10.1016/j.joule.2019.12.018.
[36] Costantino A, Comba L, Sicardi G, et al. Energy performance and climate control in mechanically ventilated greenhouses: a dynamic modelling - based assessment and investigation. Appl Energy 2021;288:116583. https://doi.org/10.1016/j.apenergy.2021.116583.
[37] Lin D, Dong Y, Ren Z, et al. Hierarchical optimization for the energy management of a greenhouse integrated with grid-tied photovoltaic-battery systems. Appl Energy 2024;374:124006. https://doi.org/10.1016/j.apenergy.2024.124006.
[38] Abdolrasol M, Ayob A, Lipu M, et al. Advanced data - driven fault diagnosis in lithium-ion battery management systems for electric vehicles: progress, challenges, and future perspectives. eTransportion 2024;22:100374. https://doi.org/10.1016/j.etran.2024.100374.
[39] Wang L, Zhang Y, Li Z, et al. P2P trading mode for real-time coupled electricity and carbon markets based on a new indicator green energy. Energy 2023;285:129179. https://doi.org/10.1016/j.energy.2023.129179.
[40] Wang J, Zhong H, Yang Z, et al. Exploring the trade-offs between electric heating policy and carbon mitigation in China. Nat Commun 2020;11:6054. https://doi.org/10.1038/s41467–020-19854-y.
[41] Wang Q, Wu W, Lin C, et al. An exact relaxation method for complementarity constraints of energy storages in power grid optimization problems. Appl Energy 2024;371:123592. https://doi.org/10.1016/j.apenergy.2024.123592.
[42] Chen S, Yoo S, Fang Y. Quantum long short-term memory. IEEE international conference on acoustics, speech and signal processing (ICASSP). 2022. p. 8622–6. https://doi.org/10.1109/ICASSP43922.2022.9747369.
[43] Zhang K, Bai D, Li Y, et al. Robust state-of-charge estimator for lithium-ion batteries enabled by a physics-driven dual-stage attention mechanism. Appl Energy 2024;359:122666. https://doi.org/10.1016/j.apenergy.2024.122666.
[44] Ajagekar A, You F. Quantum computing for energy systems optimization: challenges and opportunities. Energy 2019;179:76–89. https://doi.org/10.1016/j.energy.2019.04.186.
[45] Wang D, Zheng K, Teng F, et al. Quantum annealing with integer slack variables for grid partitioning. IEEE Trans Power Syst 2023;38(2):1747–50. https://doi.org/10.1109/TPWRS.2022.3229862.
[46] Mastroianni C, Plastina F, Scarcello L, et al. Assessing Quantum Computing Performance for Energy Optimization in a Prosumer Community. IEEE Trans Smart Grid 2024;15(1):444–56. https://doi.org/10.1109/TSG.2023.3286106.
[47] Wang L, Weng Z, Li R, et al. Collaborative operational model for shared hydrogen storage and energy prosumers:a quantum game approach. Int J Hydrog Energy 2026;204:153266. https://doi.org/10.1016/j.ijhydene.2025.153266.
[48] Zheng W, Xiao H, Pei W. Distributed-regional photovoltaic power generation prediction with limited data: a robust autoregressive transfer learning method. Appl Energy 2025;380:125058. https://doi.org/10.1016/j.apenergy.2024.125058.
[49] Zhou Z, Dai Y, Leng M. A photovoltaic power forecasting framework based on attention mechanism and parallel prediction architecture. Appl Energy 2025;391:125869. https://doi.org/10.1016/j.apenergy.2025.125869.